Engineering Structures 183 (2019) 70–82

Contents lists available at ScienceDirect

Engineering Structures

journal homepage: www.elsevier.com/locate/engstruct

Influence of masonry infills on seismic response of RC frames under low frequency cyclic load

Ning Ning[a,b,c,*], Zhongguo John Ma[c,d], Pengpeng Zhang[e], Dehu Yu[a,b], Jianlang Wang[a,b]

[a] School of Civil Engineering, Qingdao University of Technology, 11Fushun Rd, Qingdao 266033, China
[b] Collaborative Innovation Center of Engineering Construction and Safety in Shandong Blue Economic Zone, Qingdao 266033, China
[c] Department of Civil and Environmental Engineering, the University of Tennessee Knoxville, TN 37996-2313, USA
[d] Visiting Prof., School of Civil Engineering, Southwest Jiaotong University, Chengdu 610031, China
[e] School of Civil Engineering, Xi'an University of Architecture and Technology, Xi'an 710055, China

ARTICLE INFO

Keywords:
Aerated lightweight concrete (ALC) blocks
infills
RC frames
Seismic response
Interaction force
Equivalent strut

ABSTRACT

This paper presents an investigation on the seismic behavior of four reinforced concrete (RC) frames. The study is focused on the effect of the Aerated Lightweight Concrete (ALC) blocks infills on the seismic performance of the RC frames and the interaction between infills and surrounding frames. Four RC frames include a control specimen, frame with full-filled infills, frame with large window openings, and frame with eccentric door openings. Based on the low frequency cyclic loading experiments, hysteretic dissipation ability, stiffness degradation, characteristic displacement and load, failure pattern, flexural moments of columns, effective slab width, required ratio of column-to-beam strength, and column shear force are experimentally investigated and analyzed. Tests results indicate that the strength, the initial stiffness and the area of the hysteretic loop at the same load step were influenced significantly by infills when compared with the frame without masonry infills. This effect was reduced due to the large openings in the frame with infills. The column and beam mixed hinges failure was observed in the frame without infills while shear failure appeared at column ends in frames with infills. The testing results also show that inflection points were shifted to columns top because of the infills. Column shear forces were increased significantly due to the diagonal strut effect. Recommendations on useful effective slab width, the required ratio of column-to-beam strength and the equivalent strut width are made to take masonry infills into consideration in design.

1. Introduction

Masonry infills are frequently used in reinforced concrete (RC) structures. Since they are normally considered as architectural elements, the role of infills is underestimated in design code [1-4]. Seismic damage investigation indicated that RC frames were damaged showing "strong beam-weak column" failure, shear failure, and joint failure, which went against the original design intention. During strong earthquakes, the majority of RC frames collapsed or suffered a soft story failure due to few infills in the first floor (Fig. 1) [5]. Disproportionate openings led to short-column shear failure (Fig. 2) [6]. These damages illustrate that the infills have a significant effect on the whole structure and cannot be ignored. Thus, more researches should be carried out to understand the role of infills during strong earthquakes.

During the last few decades, experimental studies on RC frames with masonry infills under static loads were carried out. Around 1960s, Polyakov [7] and Holmes [8] first found that brick infills could increase the strength and stiffness of frames, which brought infills effect into the sight of researchers. In order to compare seismic performance of RC frames with different infill materials and load routines, Bertero [9] carried out quasi-static cyclic load and monotonic load tests of 1/3 scaled 3-1/2 stories frames, Bertero [9] pointed out that the initial lateral stiffness, maximum lateral resistance, and effective viscous damping coefficient of frames increased significantly due to the effect of infills. Zovkic [10] also pointed out that the seismic performance was greatly influenced by the material of the infills. Armin [11] considered other influence factors such as strength of infills with respect to bounding frames, panel aspect ratio and vertical loads. After testing twelve 1/2 scaled frames, Meharbi [12] concluded that in addition to infills effect on strength and stiffness of structures, strong frames and strong panels exhibited a better performance in terms of load resistance and energy-dissipation capacity while shear failure appeared in columns in weak frames and strong panels. These results are important to gravity load designed frames.

* Corresponding author at: School of Civil Engineering, Qingdao University of Technology, 11Fushun Rd, Qingdao 266033, China.
E-mail address: ningning8226@icloud.com (N. Ning).

https://doi.org/10.1016/j.engstruct.2018.12.083
Received 4 September 2018; Received in revised form 24 December 2018; Accepted 27 December 2018

Fig. 1. Soft story failure [5]

Fig. 2. Shear failure of short column [6]

In order to study infills with openings, Sigmund [13] carried out ten 1:2.5 scaled frames with windows and doors by considering the location of openings and tie-columns. Sigmund [13] found that tie-columns increased the system ductility. Sigmund [13] also pointed out that openings did not influence the initial stiffness and strength at low drift levels, which was contrary to the existing research results [14]. Stavridis [15] concluded that more damage appeared in infills with openings than those without openings after the shaking table tests of 3 story 2 bay 2/3 scaled frames with infills.

In addition to the effect of infills on strength and stiffness, it was found that infills could transfer forces to beams, columns and connections. Also, the bracing of frame members across a patial length was found important. Sucuoğlu [16] tested one frame with AAC (Autoclave Aerated Concrete) blocks by pseudo-dynamic method and pointed out that shear transferred from the AAC panel to the boundary column needs to be accounted for in design. Calculation method of capacity shear of the boundary column was proposed. Siddiqui [17] pointed out that infill walls tend to localize damage at the critical story due to a peculiar frame-infill interaction, and to impose larger internal force and deformation demands on the columns and beams bounding the infills by the pseudo-dynamic procedure of a 3-storey, 3-bay frames specimen with infills in the middle span. Buonopane [18] investigated moments and axial forces in the frame columns via a pseudo dynamic testing of RC frames with infills. Infills effect on axial force, shear force and shear in beam-column joints was investigated by Haldar [6] using SAP2000.

The effect of infills and frames can be expressed as a diagonal strut. Single equivalent strut model of infills was first proposed by Polyakov [7] based on the testing data. In the following investigations [19,20], different equivalent strut widths recommended due to infill crack which lead to a quick decrease of structure. Multiple-strut model for infills was proposed by Chrysostomou [21], El-Dakhakhni [22,23] with a higher degree of accuracy. Those research results indicated that the strut width was related to stiffness of frames and infills which was accepted by ASCE41-06 [2]. However, multiple-strut models for infills without openings and with openings [18] are complex and not convenient in design.

In summary, different influence factors have been considered in the existing experiments. The main research results are that infills can influence stiffness, strength, and energy dissipation ability of structures significantly. However, research data on RC frames with openings especially large openings and eccentric openings are limited. Interaction between infills and surrounding frames such as effect on shear failure of columns, column moment, axial load was investigated, but testing data and analysis is still insufficient. Effective slab width and required ratio of column-to-beam strength which is important to achieve strong column and weak beam have rarely been studied.

ASCE41-06 points out that “theoretical work and experimental data for determining multiple strut placement and strut properties, however, are not sufficient to establish reliable guidelines”. Multiple strut models for infills with openings, especially for eccentric openings are not ready for implementation. Ignoring or underestimating the interaction between infills and surrounding frames in design might result in the “strong beam-weak column” or “strong bending-weak shear” failure. The objective of this paper is to study the seismic performance of the RC frames with infills as well as the interaction of infills and surrounding frames. Low frequency experiments on bare frame, full-filled infilled frame, frame with eccentric door openings and frame with large window openings were performed. The test results should provide the insight on the role of infills in RC frames especially the infills effect on the frame component during strong earthquakes and enrich testing data for computing models of infills. Simplified strut model for infills with and without openings is proposed in this paper based on testing data.

2. Experimental investigation

2.1. Material properties

Ordinary Portland cement was used in this study. The water-to-cement ratio was 0.45. The average compression strength and elastic modulus was tested by 150 mm × 150 mm × 150 mm concrete cubes and 100 mm × 100 mm × 300 mm concrete prisms, respectively.

Aerated Lightweight Concrete (ALC) blocks with excellent characteristics of thermal insulation are light weight. ALC blocks can substitute for clay brick as green building materials in the future. ALC blocks have been widely used in RC frames in China. Because of its low compressive strength, the role of ALC infills was underestimated. Therefore, it is important to study ALC the effect of infills on seismic performance of RC frames. 240 mm × 120 mm × 100 mm ALC blocks were cut to fit the testing specimens. 70.7 × 70.7 mm × 70.7 mm mortar cubes were made to determine the compressive strength of mortar. Material properties of concrete, ALC and mortar are shown in Table 1.

Reinforcement with diameters of 6 mm, 8 mm and 12 mm was used as the slab bars and stirrups, beam longitudinal bars and column longitudinal bars, respectively. Steel wires of 4 mm diameter were used as connect bars. The yield strength, tensile strength and elastic modulus of steel bars are classified in Table 2. The spacings of lateral reinforcement of beams and columns are shown in Fig. 3(f). The provision of Chinese code for stirrup ratio and longitudinal reinforcement ratio is shown in the Table 3. Please note that the scaled model was used for testing, no appropriate diameter of steel bar is available. Thus, the frames were designed to satisfy the minimum stirrup ratio.

Table 1
The properties of concrete, ALC and mortar.

Location	Concrete		ALC	Masonry units	Mortar
	Compressive strength/MPa	Elastic modulus /10e^4	Compressive strength/MPa	Compressive strength/MPa	Compressive strength/MPa
1st story	28.8	2.85	1.64	2.38	13.87
2nd story	27.1	2.79			

2.2. Model description

The experimental work consisted of four 1:2.5 scaled RC frames: a control specimen (RC-0), RC frame with full-filled infills (MRC-1), RC frame with door-openings infills (MRC-2) and RC frame with window-openings infills (MRC-3). All specimens were made of main beams with a cross section of 100 mm × 200 mm, transverse beam with a cross section of 100 mm × 150 mm and columns with a cross section of 160 mm × 160 mm. The thickness of slabs is 50 mm. The span of the frames is 2.4 m. The height of the frame is 2.88 m (each floor with the height of 1.44 m). The frames were designed according to the Chinese concrete structure code (GB50010-2010). Fig. 3 shows the geometry of the frames and the details of the specimens. According to Chinese code [3], two connect bars with a minimum diameter of 6 mm and a length of 500 mm should be used at every 500 mm-600 mm spacing along the infilled wall height. After scaling, the connecting bar length of 200 mm was used in every 2 wythe blocks. Fig. 4 shows the construction of the infills and set up of the connection bars.

2.3. Load setup and instrumentation

Load cell mounted in the actuator was used to record the lateral loads. Linear Variable Differential Transducers (LVDTs) were mounted on each floor of the frames as well as base to monitor the lateral displacements. Strain gauges were attached to the steel bar of columns, beams and slabs to measure the strain of reinforcement (Fig. 5).

The overall view of loading setup is shown in Fig. 6. The top of the frames was connected to L shaped steel beam on which the axial load was applied by a hydraulic jack. Lateral load was applied to the L shaped beam by a servo actuator. L shaped beams were connected to the steel frame by a four bar linkage to realize lateral free movement. The push direction is defined as the positive direction, namely east to west.

2.4. Loading program

The tests were carried out at Structure Laboratory of Qingdao University of Technology. The lateral load was applied by a 100 t servo actuator. Vertical load was applied by a 50 t hydraulic jack. The axial load ratio was 0.2. The vertical load was applied at the middle of steel beam of the loading frame. However, 30 mm concrete pads were fixed at the top of the columns to make sure that the vertical loads were transferred by the columns only. The vertical load on the top of each column is 36.6 kN. The variation of the axial loading during the test was ± 1\% of the applied load.

The whole tests were controlled by displacement. At the beginning of the test, 1 mm displacement was applied to check the instruments. The load routine was 0.05% story drift (1.5 mm) → 0.1% story drift (3 mm) → 0.16% story drift (4.5 mm) → 0.2% story drift (6 mm) → 0.26% story drift (7.5 mm) → 0.3% story drift (9 mm) → 0.4% story drift (12 mm) → 0.6% story drift (17 mm) → 0.8% story drift (23 mm) → 1% story drift (29 mm) → 1.25% story drift (36 mm) → 1.5% story drift (43 mm) → 2% story drift (58 mm) → 2.5% story drift (72 mm) → 3% story drift (86 mm) → 3.5% story drift (101 mm) → 4% story drift (110 mm). Except 0.05% story drift, each load step was repeated 3 times to consider the stiffness degradation. Due to obvious reduction of carrying capacity, testing of four frames ended at different displacements. The loading routine is shown in Fig. 7.

3. Seismic performance of frames

3.1. Observed response

3.1.1. Specimen RC-0

Hair cracks appeared on columns and beams at 0.1% story drift while cast in-situ slabs did not crack till 0.6% story drift. With increase of lateral displacement, new cracks appeared and became wider. After 2% story drift, reaching the peak lateral load of 36.28kN, most of existing cracks widened while few new cracks were observed. When the story drift reached 2.5% with the lateral load of 36.0kN, transverse beam began to crack. In the slab-in-tension case, cast-in-situ reinforcement lead to torsion failure of transverse beams and the concrete of transverse beam peeled off (Fig. 5(a)). The crack width of east beam at the first floor was more than 5 mm and plastic hinge formed (Fig. 5(b)). Concrete of column feet was crushed at the last few steps of test (Fig. 8(c)).

3.1.2. Specimen MRC-1

Cracks formed early on infills, with the story drift and average lateral loading of 0.16% and 18.98kN, respectively. Columns and beams cracked at 0.2% story drift while cracks appeared at cast-in-situ slabs at 0.3% story drift. Cracking sound of infilled walls was heard at 1% story drift. After that, cracks widened immediately and 45 degree diagonal cracks formed, reaching an average lateral loading of 83.84kN. After 1.25% story drift with the average lateral load of 87.61kN, torsional crack appeared on transverse beams near joints. The west joint failure occurred at 2.5% story drift with the average lateral load of 95.9kN. However, only a few new cracks appeared after 2.5% story drift. Shear failure occurred at the column top of the first floor (Fig. 9(a)). At 2.5% story drift, the connecting bars between infills and columns were pulled out (Fig. 9(b)). The contact length between infilled wall and column was approximately 100 mm at 3.5% story drift. At the end of the test, torsion-crack widths of transverse beams were more than 10 mm (Fig. 9(c)), Column feet concrete was crushed (Fig. 9(d)), and the

Table 2
The properties of reinforcement.

Reinforcement	Diameter (mm)	Yield strength (MPa)	Tensile strength (MPa)	Elastic modulus (10^{5}MPa)
Connection bars	4	512	609	2.06
Slab bars and Stirrups	6	303	344	1.81
Beam longitudinal bars	8	311	459	1.56
Column longitudinal bars	12	403	583	2.02

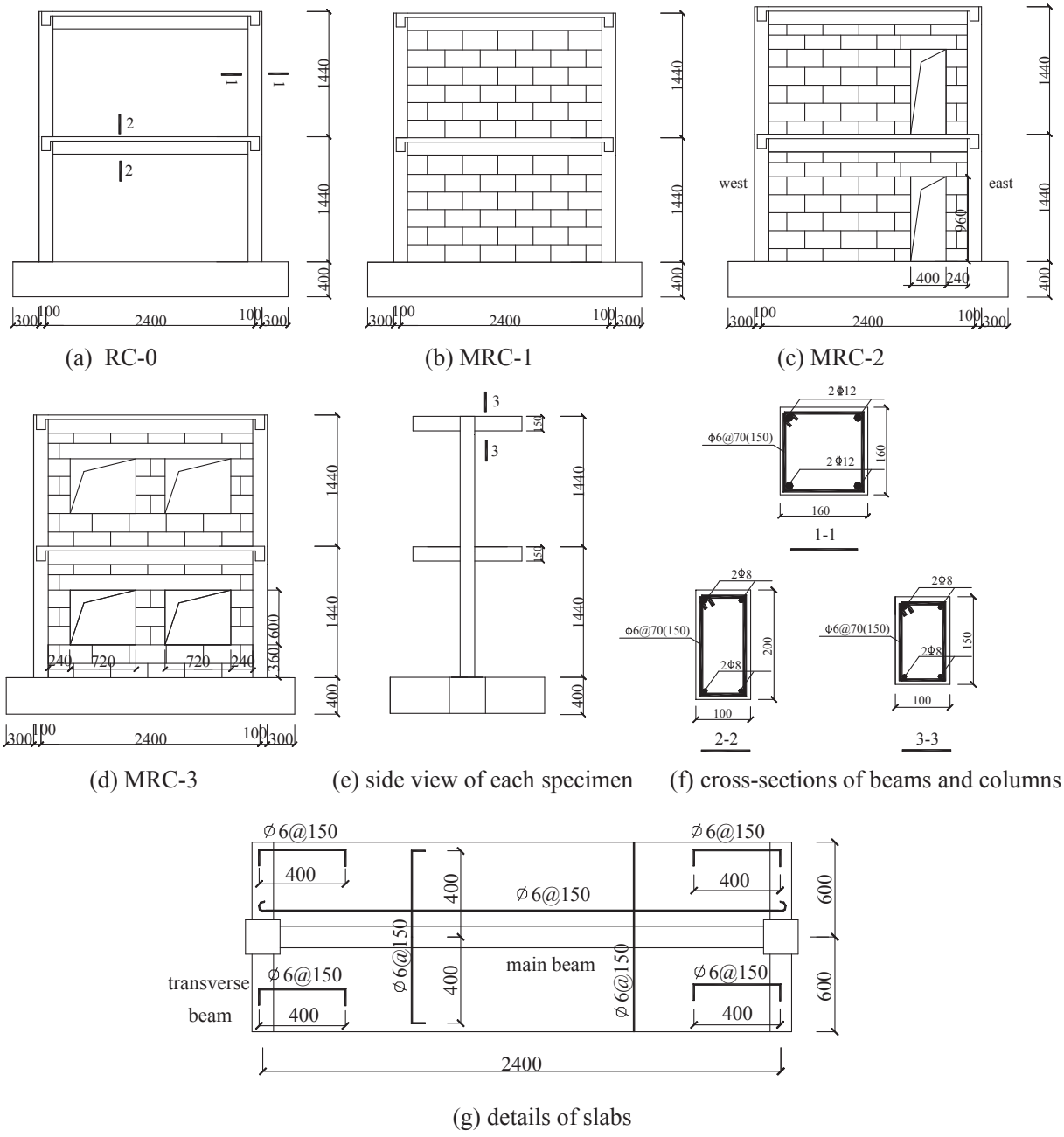

Fig. 3. Details of specimens.

diagonal struts were observed on infills (Fig. 9(f)).

3.1.3. Specimen MRC-2

Cracks appeared at beams ends at 0.16% story drift. Sudden diagonal cracks appeared on west side of infilled walls at 0.2% story drift, with the average lateral loading of 45.8kN. The length of the diagonal cracks is 1 m. The cracks on infilled walls were broadened when the displacement reached 0.3% story drift and 0.6% story drift, with the average lateral load of 55.8kN and 72.5kN, respectively. Cracks appeared on cast-in-situ slabs, transverse beam and joints at 0.3%, 0.8% and 1% story drift, with the average lateral load of 55.8kN, 72.0kN and 75.3kN, respectively. At the 2.5% story drift, west joint suffered shear failure. Shear failure occurred at the top of the first floor column (Fig. 10a)). At the end of the test, the infilled walls almost fell down (Fig. 10(b)).

Table 3
The stirrup ratio and longitudinal reinforcement in ratio of specimens.

Component	Minimum stirrup ratio	Stirrup ratio of testing frames	Minimum of longitudinal reinforcement ratio	Maximum of longitudinal reinforcement ratio	Longitudinal reinforcement ratio of testing frames
beam	0.14%	0.8%	0.22%	2.5%	0.5%
column	0.35%	1.8%	0.7%	5%	1.7%

Fig. 4. Connect bars of infills.

3.1.4. Specimen MRC-3

Cracks appeared on columns and beams at 0.1% story drift, at the same time infilled walls cracked, reaching the lateral loading of 17.65 kN. Cracks appeared at cast in-situ slabs at 0.3% story drift. When the displacement reached 1% story drift with the average lateral load of 53.7 kN, cracks appeared on transverse beams near joints. Increasing number of cracks appeared on columns at 1.5% story drift (average lateral load of 57.3 kN). Column shear cracks appeared near joints accompanied by loud noise (Fig. 11(a)). Lintels above the windows almost fell down and infills between window-openings destroyed (Fig. 11(b)–(c)). Diagonal cracks also appeared in the middle of first floor columns (Fig. 11(d)). 45 degree diagonal cracks were observed at the corners of windows.

3.1.5. Comparison of the specimens

Slab cracks appeared at 0.6% story drift for RC-0 while cracks appeared at 0.3% story drift for MRC-1, MRC-2 and MRC-3, which indicated that infilled walls led to a early crack of slabs. Cracks were observed at columns at 0.3% story drift for MRC-1 while cracks appeared at columns at 0.1% story drift for RC-0, which showed that cracks at columns could be delayed due to infills. Diagonal cracks appeared on columns of specimens with infilled walls, which illustrated the potential shear failure of columns.

The diagonal crack in RC-0 was extended to almost whole transverse beam while cracks of MRC-1 were within the scope of one transverse beam height. This phenomenon indicated that the participation of slabs reinforcement in tension was decreased due to infilled walls. The width of main diagonal cracks at joints of MRC-1 is wider than 10 mm, which indicated that shear forces transferred to joints are larger due to infilled walls.

45 degree diagonal cracks of infill walls appeared at the first few steps of the tests and strut formed early, which indicated that a strut model deduced by elastic theory may not be suitable. The top corners of the infills in MRC-1 were crushed at large displacements, which caused shear failure of the extremely short column. Cracks at the corners of the doors and windows were along approximately 45 degree direction. Infills under the lintel were crushed and the lintel was almost disengaged from infills.

3.2. Hysteretic loops

The hysteretic loops are shown in Fig. 12. Before reinforcement was yielded, the curves are approximately linear, and areas of hysteretic loops of each frame are small, which indicated that the energy absorbed by specimens was relatively small. At the nonlinear stage, the shape of the hysteristic loops became different: RC-0 was fusiform while MRC-1 was inverse sigmoid curve shape. Comparing with RC-0, the area of hysteretic loops of MRC-1 was larger at the same displacements, which indicated a larger energy absorption of MRC-1. The curve shape of

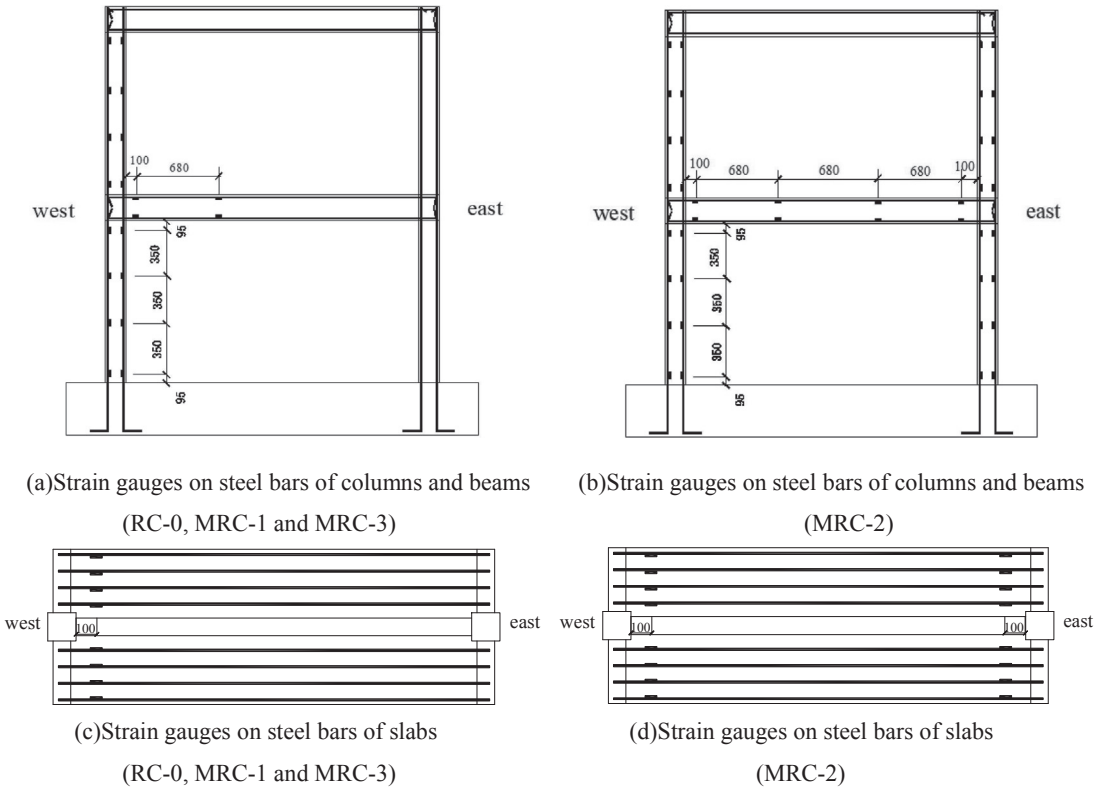

Fig. 5. Locations of strain gauges.

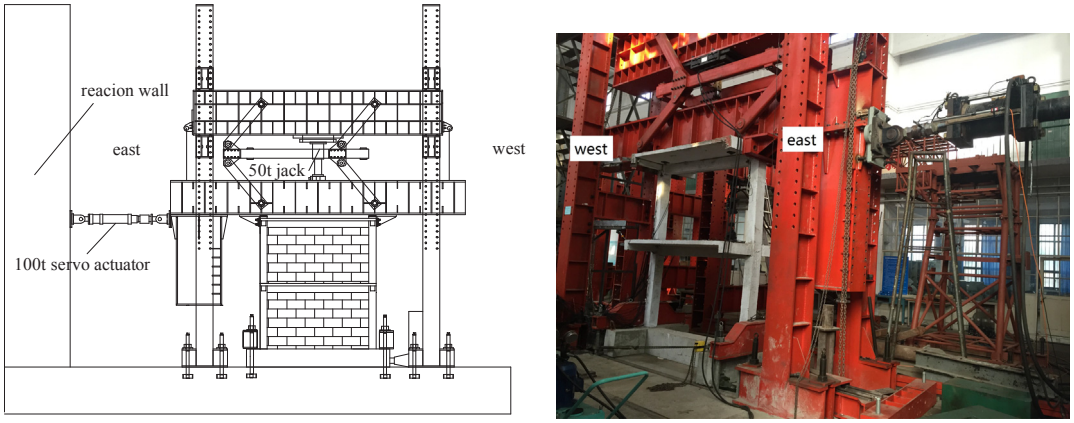

(a)Elevation view (b)The set up photo of RC-0

Fig. 6. Loading setup.

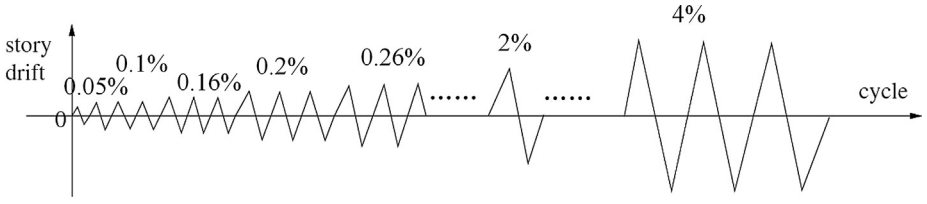

Fig. 7. Loading Routine.

MRC-2 was similar to MRC-1 while the curve shape of MRC-3 was similar to RC-0, which illustrated that the area of openings effected on the energy absorption of specimens.

3.3. Skeleton curve

The skeleton curves of lateral load (P)- top displacement (Δ) are shown in Fig. 13. Values were extracted from the first circle of each loading step. It is shown that in the elastic stage, the skeleton curves are linear. The curves show non-linearity in the elastic-plastic stage. After the peak loads, the carrying capacity decreases with the increase of lateral displacement.

It can also be indicated that infills played an important role on the strength of specimens. Lateral loading of MRC-1 dropped faster after the peak load than the decline period of RC-0. The average peak load and corresponding displacement of RC-0 are 36.28kN and 57.78 mm while those of MRC-1 are 89.76kN and 46.68 mm, respectively. Infilled walls of MRC-1 resulted in a 1.47 time higher peak load as well as 80.79% of corresponding displacement than those of RC-0. Specimens showing peak loads from high to low are MRC-1, MRC-2, MRC-3 and RC-0, which indicated that infills increased the strength of the structures while the area of openings influenced the strength of specimens. Area of openings also influenced the shape of the skeleton curve. The shape of skeleton curve of MRC-3 was similar to that of RC-0.

3.4. Stiffness degradation

The stiffness degradation curves are shown in Fig. 14, which shows that infills had a significant influence on initial stiffness of frames. The initial stiffness of MRC-1 was 3.56 times larger than that of RC-0 in the positive direction. The negative direction stiffness of MRC-2 was almost the same as MRC-1 while positive direction stiffness of MRC-2 was much smaller than that of MRC-1 due to asymmetrical opening. Although existing large openings, the initial stiffness of MRC-3 was 1.64 times larger than that of RC-0 in positive direction. The stiffness was degenerated with the increase of displacement. At the end of tests, the stiffness of four frames were close.

3.5. Characteristic displacement and load

Table 4 shows the characteristic values of the specimens. P_y, P_{max} and P_u are the yield load, peak load and ultimate load (85% of the peak load), respectively. P_y was calculated by using the energy equivalent method. These loads are defined as the average load of the positive and

(a) failure of transverse beam (b) beam hinge (c) crushing of column foot

Fig. 8. Cracks of RC-0.

(a) crushing of infills and shear failure of column (b)pulled out of connect bars (c) transverse beam failure

(d) crushing of column foot (e) failure of joint (f) diagonal cracks of infilled walls

Fig. 9. Cracks of MRC-1.

(a) failure of joint and column (b) failure of infilled walls

Fig. 10. Cracks of MRC-2.

(a) diagonal crack at column top (b) Lintel above the windows

(c) infills between windows (d) diagonal cracks at columns

Fig. 11. Cracks of MRC-3.

negative directions. It can be concluded that infills have an obvious effect on the lateral load of specimens. P_y, P_{max} and P_u of MRC-1 are 153.63%, 147.41%, and 147.37% higher than those of RC-0, respectively. The values decrease with the increase of the area of openings. RC frames with infills have a higher strength than RC frames without infills.

Δ_y, Δ_{max}, and Δ_u are the yield displacement, peak displacement, and ultimate displacement, respectively. MRC-2 is characterized by the lowest displacement, probably due to the asymmetrical opening. The yield displacement, peak displacement, and ultimate displacement of RC-0 are 142.52%, 35.03%, and 56.26% higher than those of MRC-2, respectively.

The deformation ability of specimens is reflected by displacement ductility coefficients, which are defined as ultimate displacement divided by yield displacement, as well as by the ultimate story drift, which is defined as ultimate displacement divided by height of frames (H). Table 4 also shows that all the specimens have good deformation abilities.

3.6. Failure patterns

The location of hinges and shear failure of columns are shown in

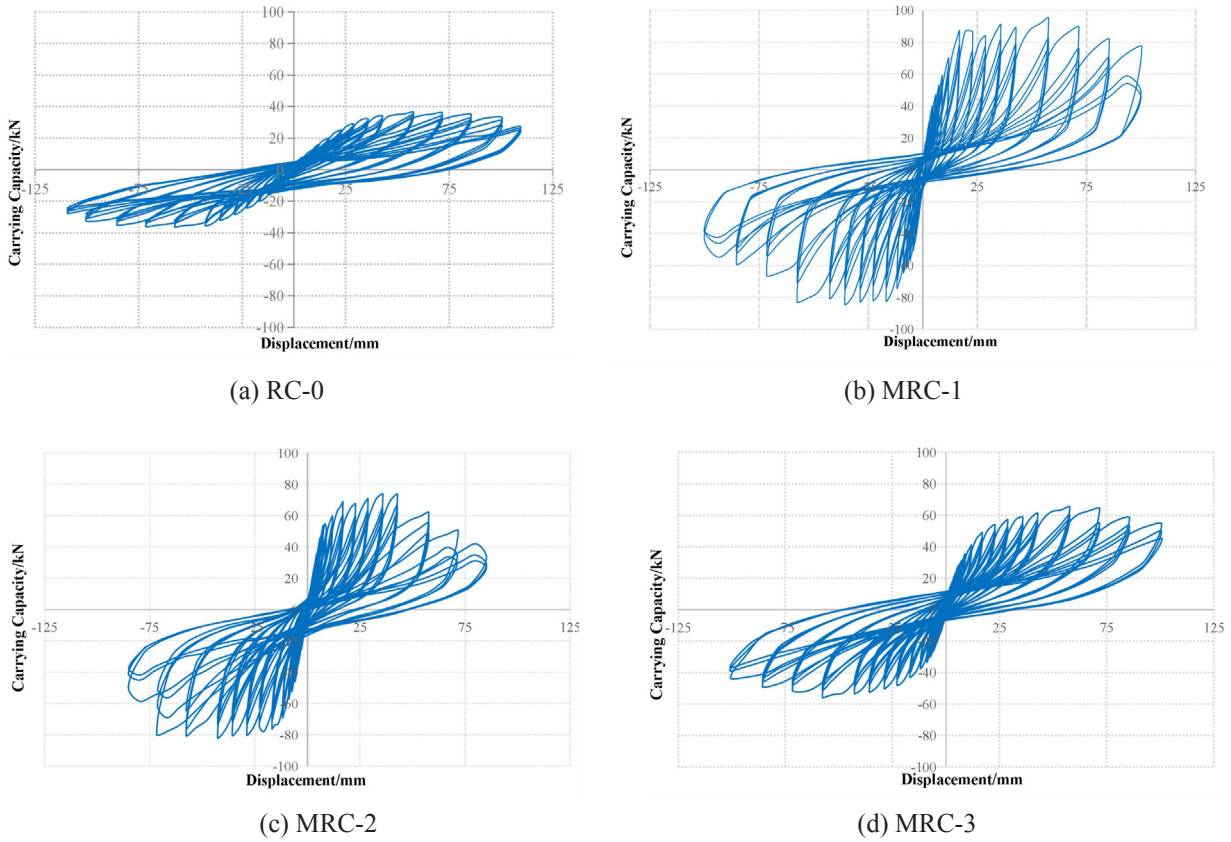

Fig. 12. The hysteretic curves.

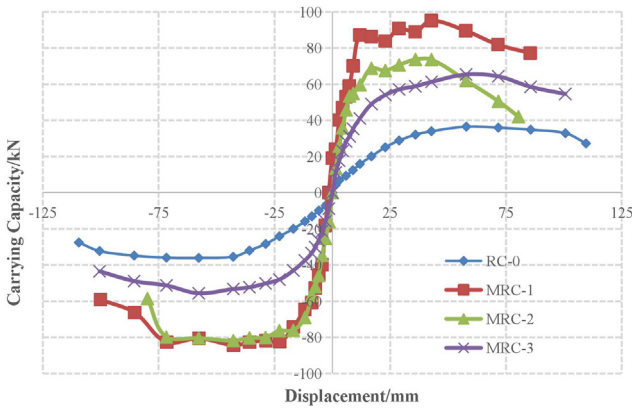

Fig. 13. The skeleton curves.

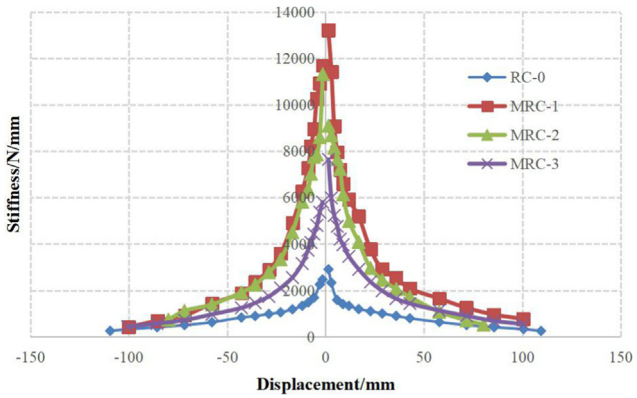

Fig. 14. The stiffness degradation curves.

Fig. 15. The column and beam mixed hinges failure was observed in RC-0. Plastic hinge first appeared at east beam end of the first floor. At the end of the test, column-foot hinges formed in both columns.

Shear failure appeared in columns of MRC-1. After diagonal cracks appeared at infilled walls, diagonal cracks appeared at the first floor column top. As soon as the corner infills was crushed, shear crack developed rapidly, which led to shear failure of the column top. Similar phenomenons were observed in MRC-2 and MRC-3. Infills effect on shear forces of columns should be taken into consideration in design.

4. Analysis of test result

4.1. Rotation of columns and beams

Rotations of the west column feet and west beam ends of the first floor within 2% story drift are shown in Fig. 16. It is found that infills restrained the rotation of the columns, which may have an effect on the flexural moments and locations of inflection points (see more details in Sections 4.4 and 4.5). MRC-1 has the smallest rotation of the column feet because of lack of openings. At the beginning of the testing, the beam rotation of RC-0 was slightly larger than other three specimens. In large displacement, this phenomenon was not obvious probably because of the gap between beams and infills due to abscission of mortar or crushing of infills which caused the concentrated deformation at beam ends.

4.2. Slab longitudinal reinforcement strain and effective slab width

The strains of slab reinforcement were obtained by embedded strain gauges. Fig. 17 shows the strain variation of top and bottom longitudinal reinforcements at 2% story drift (slab under tension during the first cycle of each loading step). It can be found that the strain value decreased with the increase of the distance from columns. Most of the

Table 4
Characteristic displacement and load.

Specimen	P_y/kN	Δ_y/mm	P_{max}/kN	Δ_{max}/mm	P_u/kN	Δ_u/mm	$\mu = \Delta u/\Delta y$	$R_u = \Delta_u/H$
RC-0	31.53	34.39	36.28	57.78	30.84	103.54	3.01	0.036
MRC-1	79.97	15.75	89.76	46.68	76.29	77.77	4.94	0.027
MRC-2	68.48	14.48	77.78	42.79	66.11	66.26	4.58	0.023
MRC-3	51.55	23.96	60.51	57.72	51.43	93.43	3.90	0.032

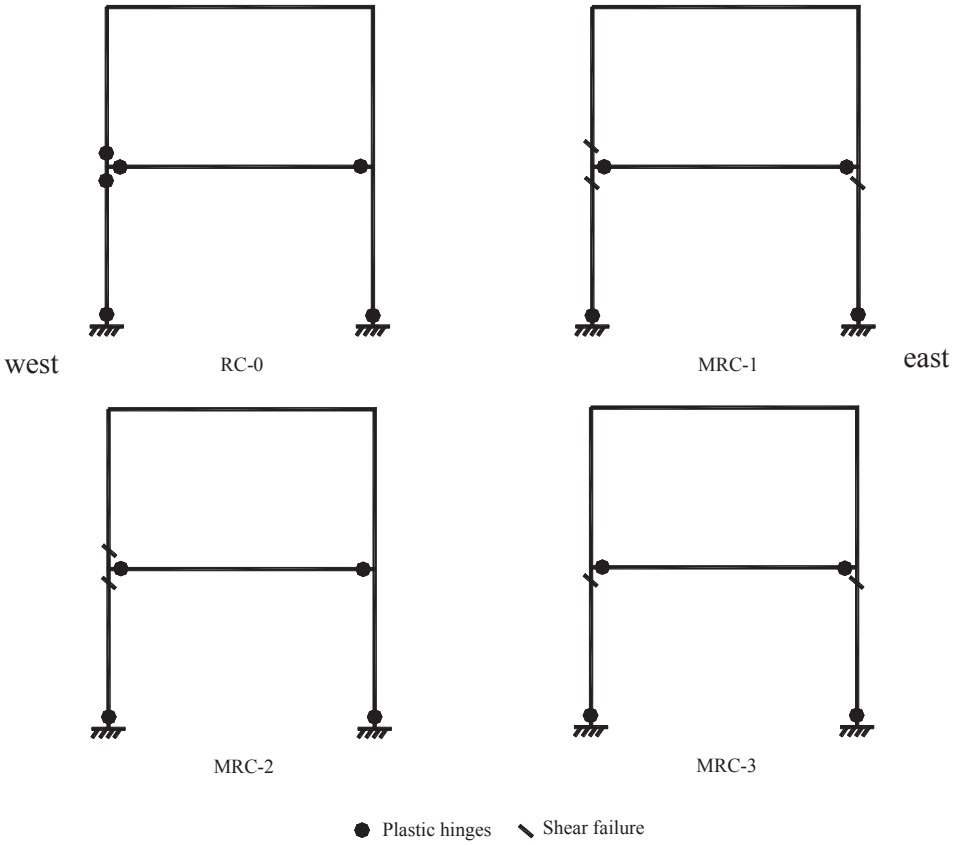

Fig. 15. Failure pattern of frames.

top reinforcement strains were larger than those of bottom reinforcement strains, which indicated that the slab top detailing reinforcement should not be ignored when calculating beam end moments.

Effective slab width is a simple and convenient method to calculate beam moments, which can be calculated using the equivalent strain method [24]:

$$b_{ef} = \frac{\int_0^x \sigma(x)dx}{\sigma_{b\,max}} + b \tag{1}$$

where $\sigma_{b\,max}$ is the maximum stress of slab reinforcement, $\sigma(x)$ is the stress of reinforcement, and b is the width of beam.

The effective slab width calculated by Eq. (1) is shown in Table 5. Effective slab width of MRC-2 west is 37% and 27% smaller than that of MRC-2 east and MRC-3, respectively, which indicates that infills can

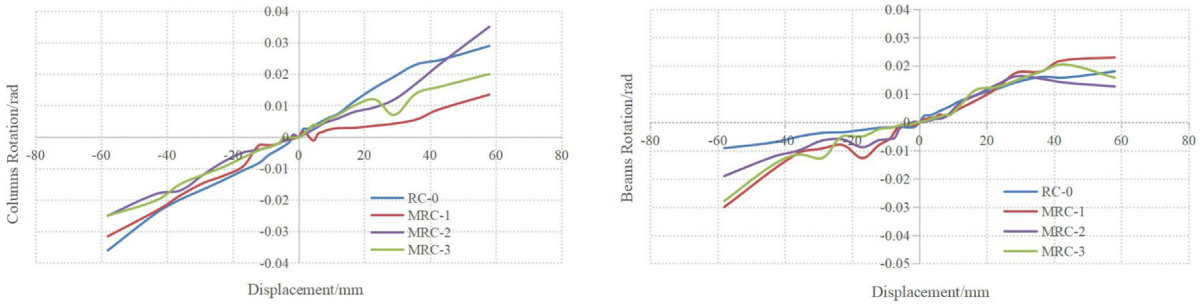

(a) Rotation of west column feet (b) Rotation of west beam ends of the first floor

Fig. 16. Rotation of columns and beams.

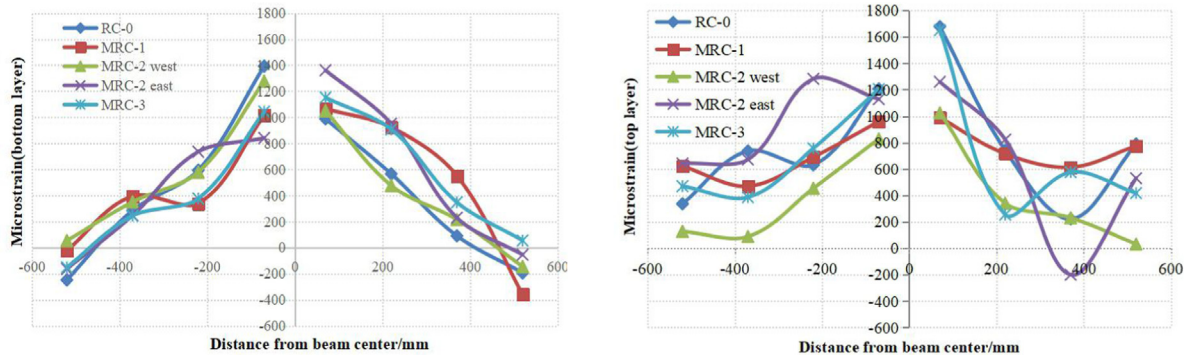

(a) Reinforcement strain at the bottom layer (b) Reinforcement strain at the top layer

Fig. 17. Strain of slab reinforcement.

Table 5
Effective slab width (2% story drift).

locations	Calculated results/mm
RC-0	389
MRC-1	423
MRC-2 west	318
MRC-2 east	436
MRC-3	404

reduce the participation of slabs and result in a smaller effective slab width. The effective slab width of MRC-1 is lager than MRC-2 west due to the crushing of infills corner which makes beams ends similar to RC-0.

ACI318-14 [4] recommends using the T-beam method to consider the effective slab width and the value calculated by ACI318-14 is 380 mm. ACI318-14 method predicts the effective slab width of MRC-2 west well, but gives larger predictions for other specimens. 300 mm effective slab width for the specimens is obtained by the EC8 [1] method. The effective slab widths calculated by ACI318-14 and EC 8 are 2.37%-14.74% and 29.67%-45.33% lower than test results, respectively. According to testing results, it is proposed that effective slab width be $b + 6.7h_s$ when slabs on both sides. Where b is the width of main beam, and h_s is the thickness of slab. Further research is needed to consider different influencing factors.

4.3. Required ratio of column-to-beam strength

The required ratio of column-to-beam strength can be defined as sum of columns moments divided by sum of beams moments calculated at 2% story drift (slab-in-tension). Slab reinforcements within the effective slab width are included in calculating beam moments.

Table 6 shows the calculated results. It can be concluded that all required ratios are less than one except for MRC-2 west. The require ratio of MRC-2 west is higher than the magnification factor of 6/5 by ACI 318-14 and close to the magnification factor of 1.3 by EC 8. According to reference [24], the required rations increase with the increase of axial compression ratio of columns. Various influencing factors will be considered in further FEM analyses. If designed by existing codes, some frames with infills will not achieve ductile failure pattern. The appropriate value should be increased in frames with infills in design.

4.4. Flexural moments of columns

Data of 0.6% story drift, which presents a medium earthquake displacement, and data of 2% story drift, which presents a strong earthquake displacement, are used to research the flextural moments along west columns of the first floor of each specimen. Columns flexural moments can be calculated by Eqs. (2)–(5) based on strain gauges measurements. The bending moment diagrams of west columns of the first floor are shown in Figs. 18 and 19.

$$e_0 = M/N \tag{2}$$

$$e = \frac{h}{2} + e_0 - a_s \tag{3}$$

$$N = \alpha_1 f_c bx + \sigma_s' A_s' - \sigma_s A_s \tag{4}$$

$$Ne = \alpha_1 f_c bx(h_0 - \frac{x}{2}) + \sigma_s' A_s'(h_0 - a_s') \tag{5}$$

where, e_0 is the eccentricity of axial load; M is the moment of columns; N is the axial load of columns; e is the distance between axial load and tension steel; a_s' and a_s are the distance from the extreme compression fiber to the compression steel, and the distance from the extreme tension fiber to the tension steel, respectively; $\alpha_1 f_c$ is compressive stress of equivalent rectangular distribution, according to Chinese code, α_1 equals to 1.0 when compressive stress of concrete below 50 MPa; f_c is compressive strength of concrete; b is the width of columns; x is the the depth of the equivalent rectangular stress block; σ_s' and σ_s are the stress of compression steel and tension steel, respectively; A_s' and A_s are the areas of compression steel and tension steel, respectively; h_0 is the effective depth.

Figs. 18 and 19 demonstrates that infills affect the location of inflection points. The inflection points are close to the top of the columns. Infills also have an influence on the moment values of column ends. At column bottoms, the moment values of MRC-1 to MRC-3 are smaller than those of RC-0 while the opposite phenomenon was observed at the

Table 6
Required ratios of column-to-beam strength.

Specimen	Moments of first floor column top/kNm	Moments of second floor bottom/kNm	Sum of columns at first floor joints/kNm	Moments of west beam ends of first floor /kNm	Required ratios of column-to-beam strength
RC-0	6.00	9.76	15.76	18.63	0.85
MRC-1	8.77	11.11	19.88	22.15	0.89
MRC-2 west	8.16	12.06	20.22	16.64	1.27
MRC-3	3.81	10.07	13.88	19.45	0.71

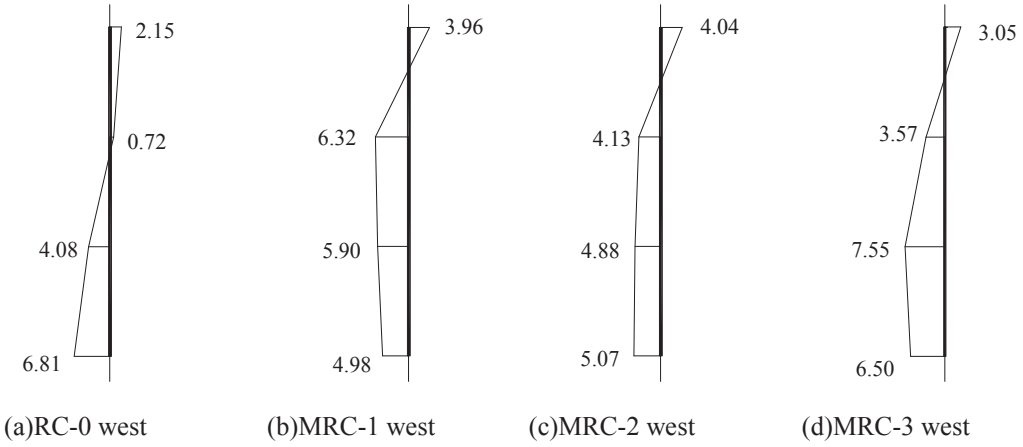

Fig. 18. Flexural moments of first floor columns (0.6% story drift) /kN·m.

top of the columns. When in tension case (west to east), the surrounding frames were separated from the infills near west lower corner and east upper corner, which caused compressive contact stresses between frames and infills as struts. The phenomenon was caused by this interaction of infills and surrounding frames and will be discussed in Section 4.5.

4.5. Analytical models of infills

ASCE41-06 and EC8 take infills as primary elements in a lateral-load- resisting system. Strut models can be divided into two catalogs: infills without openings and infills with openings. According to the testing observations, the models are shown in Figs. 20 and 23. The equivalent strut width is derived from Eqs. (6)–(15).

(1) Infills without openings (single-strut model)

The strut model is shown in Fig. 20. For the columns, the computing model of the first floor west column of MRC-1 is shown in Fig. 21, and the equations are shown in Eqs. (6)–(9)

$$\begin{cases} \sigma_s t m\frac{m}{2} + V_c m = M_{c-top} \\ V_c(H_n - m) - (a' - m)\sigma_s t(\frac{a'-m}{2} + H_n - m) = M_{c-bot} \end{cases} \quad (6)$$

$$\begin{cases} V_{c-top} = V_c + \sigma_s t m \\ V_{c-bot} = V_c - \sigma_s t(a' - m) \end{cases} \quad (7)$$

where $M_{c\text{-top}}$ and $M_{c\text{-bot}}$ are the bending moments at column top and column bottom, respectively; t is the thickness of infills; $V_{c\text{-top}}$ and $V_{c\text{-bot}}$ are the shear force at column top and column bottom, respectively; V_c is the shear force at inflection point; m is the distance from inflection point to column top; a' is the connecting length between infills and surrounding frames; H_n is the clear length of column; σ_s is the shear stress transmitted to the column.

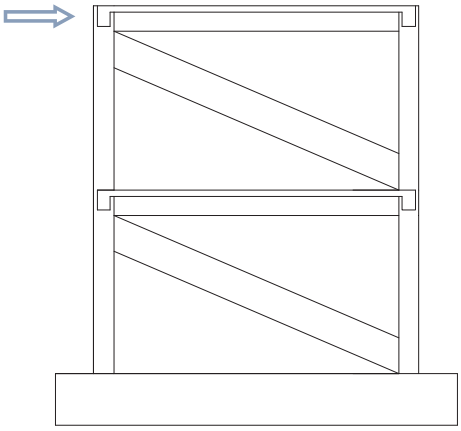

Fig. 20. Strut model of frame without openings.

According to reference [16],

$$a'\sigma_s \approx \frac{1}{2}V_s \quad (8)$$

$$V_s = a \cdot t_{inf} \cdot \sigma_{inf} \cdot \cos\theta \quad (9)$$

where, a is the equivalent strut width; t_{inf} is the thickness of infills; σ_{inf} is the compressive strength of infill; θ is the angle whose tangent is the infill height-to- length aspect ratio (radians).

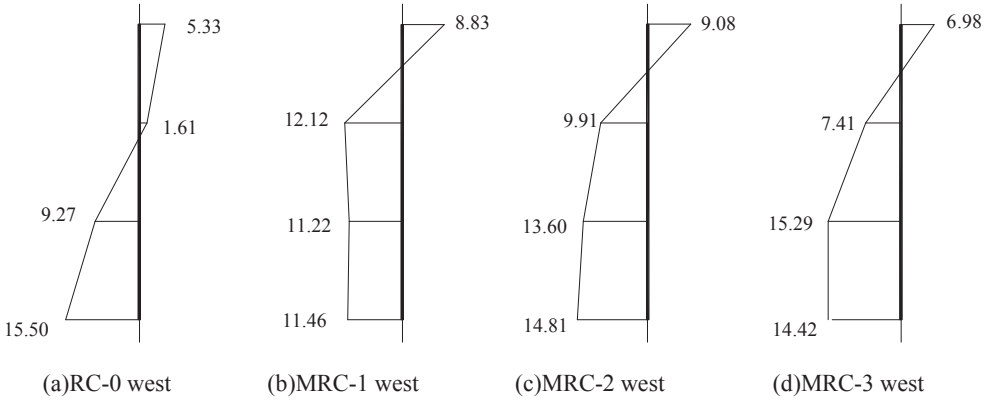

Fig. 19. Flexural moments of first floor columns (2% story drift) /kN·m.

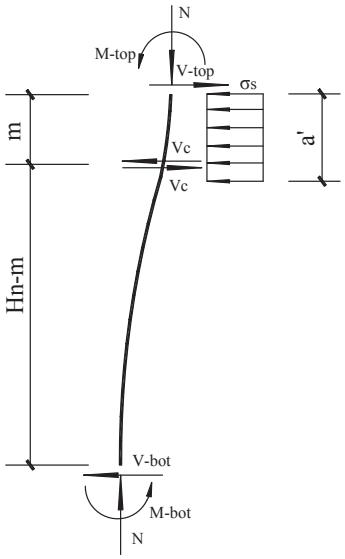

Fig. 21. The computing model of the first floor west column of MRC-1.

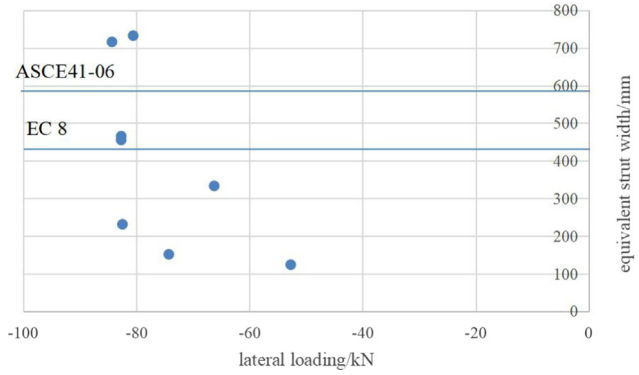

Fig. 22. Relationship of lateral force and equivalent strut width.

Equivalent strut widths in displacements of −6mm, −12 mm, −29 mm, −36 mm, −43 mm, −58 mm and −72 mm are calculated by Eqs.(6)-(9). It can be seen that the equivalent strut widths change with different lateral loadings (Fig. 22). The equivalent strut width for MRC-1 to predict the strength of frame equals to 732 mm, i.e. (1/3.5)d, where d is the strut diagonal length, comparing to the values of 511 mm and 384 mm calculated by ASCE41-06 and EC 8, respectively. The values by ASCE41-06 and EC 8 are smaller than testing result, which indicates that the values are more suitable for elastic analysis than for plastic analysis.

(2) Infills with openings (multiple-strut model)

ASCE41-06 points out that existing testings do not provide sufficient data to establish a reliable multiple strut model. Based on the crack pattern observed in this testing programme as well as on reference [18], the strut model is shown in Fig. 23. Assume that each strut has the same contact length. The calculation of the strut width of MRC-2 is similar to MRC-1. Fig. 24 shows the computing model of the first floor west column of MRC-3. For MRC-3, strut 1 has the largest strut width among struts 1, 2, and 3 (Fig. 23), thus, using the strut 1 width for design is conservative. Equivalent strut widths of MRC-2 and MRC-3 in displacements of −6mm, −12 mm, −29 mm, −36 mm, −43 mm, −58 mm and −72 mm were calculated by Eqs.(6)-(9) and Eqs.(10)-(15), respectively. The equivalent strut width for MRC-2 and MRC-3 to predict strength of frame equals to (1/3.3)d and (1/10.8)d, where d is the diagonal length of the strut. The equivalent strut width decreased with the increase area of openings, which indicates that large openings could lead to a weakened role of the diagonal effect of infills.

$$\begin{cases} \sigma_s t m\frac{m}{2} + V_c m = M_{c-top} \\ V_c(H_n - m) - (a' - m)\sigma_s t(\frac{a'-m}{2} + H_n - m) - (a' - m)\sigma_s t(n - \frac{a'}{2}) \\ \quad = M_{c-bot} \end{cases} \tag{10}$$

$$\begin{cases} V_{c-top} = V_c + \sigma_s t m \\ V_{c-bot} = V_c - \sigma_s t(a' - m) - \sigma_s t a' \end{cases} \tag{11}$$

$$a'\sigma_{s1} \approx \frac{1}{2}V_{s1} \tag{12}$$

$$V_{s1} = a{\cdot}t_{\text{inf}}{\cdot}\sigma_{\text{inf}}{\cdot}\cos\theta_1 + a{\cdot}t_{\text{inf}}{\cdot}\sigma_{\text{inf}}{\cdot}\cos\theta_2 \tag{13}$$

$$a'\sigma_{s2} \approx \frac{1}{2}V_{s2} \tag{14}$$

$$V_{s2} = a{\cdot}t_{\text{inf}}{\cdot}\sigma_{\text{inf}}{\cdot}\cos\theta_3 \tag{15}$$

where n is the height of the windowsill; θ_1, θ_2 and θ_3 are the angles of strut 1, 2 and 3 (radians); σ_{s1} and σ_{s2} are the shear stresses transmitted to the column.

It can be indicated that the values of the equivalent strut width change with parameters, such as area and location of openings. Further investigation focusing on different influencing factors will be carried

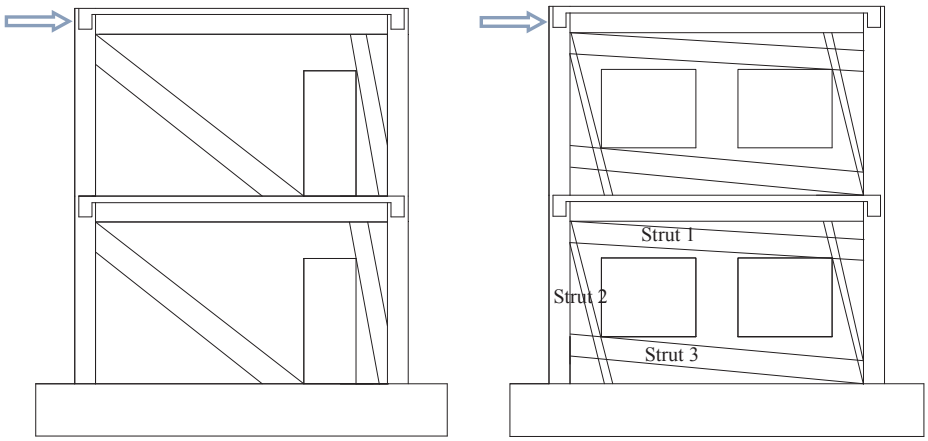

(a)MRC-2 (b)MRC-3

Fig. 23. Strut model of frame with openings.

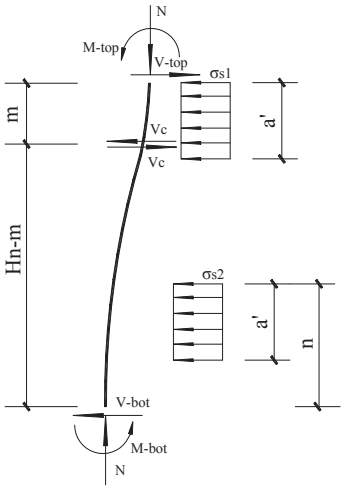

Fig. 24. The computing model of first floor west column of MRC-3.

Table 7
Maximum shear force of columns.

displacement	RC-0	MRC-1	MRC-2 west	MRC-3
−17 mm(1/150 of total height)	8.53	29.37	23.34	18.91
−58 mm(1/50 of total height)	19.84	59.86	54.26	41.11

out by FEM.

4.6. Shear force of columns

According to Eqs. (6) and (7) and (10) and (11), the maximum shear forces of west columns of the first floor appeared at column top ends (Table 7). It shows that infills had a significant influence on shear forces of columns. The largest shear force at column top appeared in MRC-1, which was 3.44 and 3.02 times of RC-0 at 1/150 and 1/50 story drift, respectively. Those shear forces decreased with the increase of openings. Shear failure may not occur on columns in medium earthquake, while it may not be reliable when the infills effects are ignored in a strong earthquake.

5. Conclusions and recommendations

Based on the four reduced-scale RC frame testing, conclusions and recommendations are summarized below.

(1) Infilled walls lead to a early crack of slabs but participation of slabs reinforcement in tension may decrease due to infilled walls. Shear failures were observed in columns near joints in RC frames infilled walls. Strut formed in infills in the early stage of loading, which indicates that the interaction between infills and surrounding frames should be taken into consideration in design.
(2) Initial stiffness and carrying capacity of RC frames were significantly increased by infills, especially full-filled infills. Openings can reduce the initial stiffness and strength of frames. At the large lateral displacement stage, as the result of cracks and crushing occurred in the infills, the lateral stiffness of four frames are almost the same. Lateral load decreased sharply after the peak load due to infills. Yield load, peak load and ultimate load are increased while yield displacement, peak displacement and ultimate displacement are decreased due to infills. Infills increased displacement ductility coefficient and decreased the story drift.
(3) Infills have an influence on the effective slab width when compared to the frame without infills. The effective slab widths ACI 318 and EC 8 are 2.37%-14.74% and 29.67%-45.33% lower than testing results, respectively. A new effective width equation was recommended with slabs on both sides according to testing results. Further models are needed to consider both slabs and infills with different influencing factors.
(4) Infills changed the flexural moments of columns as well as the location of inflection points. Infills also increased column shear forces, which led to the shear failure of column end. The effect of infills was weakened by openings.
(5) Required ratios of column-to-beam strength are calculated by testing data considering the effective slab width. The appropriate value should be increased in design. Further research is needed with different influencing factors.
(6) Models of RC frames with infills are established. Equivalent strut widths are deduced. The values are influenced by parameters such as area and location of openings.

Acknowledgments

The authors wish to acknowledge the financial support by the China National Natural Science Foundation (Grant No. 51508289 and 51478231). Special thanks are given to Mr. Weiming Ning and Mr. Baojing Huang for providing assistance to the experiments. Visiting scholar of the first author was made possible by Department of Civil and Environmental Engineering at University of Tennessee Knoxville, USA.

References

[1] European Standard EN 1998-1-2004, Eurocode 8: Design of Structures for Earthquake Resistance-Part1: General rules, seismic actions and rules for buildings. Bruxelles, Belgium:Cen, 2004.
[2] ASCE41-06:ASCE 41 Seismic Rehabilitation of Existing Buildings. ASCE, 2007.
[3] Code for design of concrete structures (GB 50011-2010) . Beijing: China Architecture and Building Press, 2010. (in Chinese).
[4] ACI Committee 318. Building Code Requirements for Structural Concrete, American Concrete Institute: Farmington Hill, HI, USA, 2014.
[5] Uva G, Porco F, Fiore A. Appraisal of masonry infill walls effect in the seismic response of RC framed buildings: a case study. Eng Struct 2012;34:514–26.
[6] Haldar P, Singh Y, Paul DK. Identification of seismic failure modes of URM infilled RC frame buildings. Eng Fail Anal 2013;33:97–118.
[7] Polyakov S.V. Masonry in Framed buildings.An investigation into the strength and stiffness of masonry infilling.Moscow, 1957.
[8] Holmes, M.. “Steel frames with brickwork and concrete infilling”. In: Proceedings of the Institution of Civil Engineers, 1961, 19(4): 473-478.
[9] Bertero V, Brokken S. Infills in seismic resistant buildings. J Struct Eng 1983;109(6):1337–61.
[10] Zovkic J, Sigmund V, Guljas I. Cyclic testing of a single bay reinforced concrete frames with various types of masonry infill. Earthquake Eng Struct Dyn 2013;42:1131–49.
[11] Mehrabi Armin B, Schuller Michael P. Asceexperimental evaluation of masonry-nfilled RC frames. J Struct Eng 1996;122(3):228–37.
[12] Meharbi AB, Shing PB, Schuller MP, Noland James L. Experimental evaluation of masonry-infilled RC frames. J Struct Eng 1996;122(3):228–37.
[13] Sigmund V, Penava D. Influence of openings, with and without confinement, on cyclic response of infilled RC frames-an experimental study. J Earthquake Eng 2014;18:113–46.
[14] Santhi Helen M, Samud Knight GM, Muthumani K. Evaluation of seismic performance of gravity load design reinforced concrete frames. J Performance Constr Facilities 2005;19(4):277–82.
[15] Stavidis A, Koutromanos I, Shing PB. Shake-table test of a 3-story reinforced concrete frame with masonry infill wall. Earthquake Eng Struct Dyn 2012;41:1089–108.
[16] Sucuoğlu H, Siddiqui UA. Pseudo-dynamic testing and analytical modeling of AAC infilled RC frames. J Earthquake Eng 2014;18:1281–301.
[17] Siddiqui UA, Sucuoglu H, Yakut A. Seismic performance of gravity-load designed concrete frames infilled with low-strength masonry. Earthquakes Struct 2015;8(1):19–35.
[18] Buonopane SG, White RN. Pseudo-dynamic testing of masonry infilled reinforced concrete frames. J Struct Eng 1999;125(6):578–89.
[19] Polyakov S. V., Holmes. On the Interactions Between Masonry Filler Walls and Enclosing Frames When Loaded in the Plane of the Wall. Moscow: Translations in Earthquake Engineering Research Institute, 1956:125.
[20] Angel R. Behavior of Reinforced Concrete Frames with Masonry Infill Walls. Department of Civil Engineering:University of Illinois at Urbana-Champaign, 1994.
[21] Chrysostomou C.Z.. “Effects of degrading infill walls on the nonlinear seismic response of two-dimensional steel frames.” PhD thesis, Cornell Univ., Ithaca, N.Y.
[22] El-Dakhakhni WW, Elgaaly M, Hamid AA. Three-strut model for concrete masonry-infilled steel frames. J Struct Eng 2003;129(2):177–85.
[23] El-Dakhakhni W. W.. “Non-linear finite element modeling of concrete masonry-infilled steel frame.” M.S. thesis, Civil and Architectural Engineering Dept., Drexel Univ., Philadelphia, 2000.
[24] Ning N, Qu W, Ma ZJ. Design recommendations for achieving “strong column-weak beam”in RC frames. Eng Struct 2016;126:343–52.